Direct fabrication of $BiFeO_3$ thin films on polyimide substrates for flexible electronics

Monika Tomczyk[1], Inigo Bretos[2], Ricardo Jiménez[2], Amit Mahajan[3], E. Venkata Ramana[4], M. Lourdes Calzada[2], Paula M.Vilarinho[1*]

[1] CICECO-Aveiro Institute of Materials, Department of Ceramics and Glass Engineering, University of Aveiro, 3810-193 Aveiro, Portugal

[2] Instituto de Ciencia de Materiales de Madrid, Consejo Superior de Investigaciones Científicas (ICMM-CSIC), Cantoblanco, E-28049 Madrid, Spain

[3] School of Engineering and Material Science, Queen Mary University of London, London, United Kingdom

[4]I3N-Aveiro, Department of Physics, University of Aveiro, 3810-193 Aveiro, Portugal

* corresponding author, e-mail: paula.vilarinho@ua.pt

Abstract

One of the major challenges for the integration of functional oxides as ferroelectrics into flexible electronics is the reduction of their processing temperature below that which causes the degradation of plastic substrates. With this aim, particular attention has been given to the low-temperature processing of oxide films by chemical solution deposition methods. In this work, lead-free multifunctional and multiferroic BiFeO3 (BFO) thin films were fabricated for the first time at a temperature as low as 300 1C directly on flexible polyimide substrates by our own proprietary solution-based Seeded Photosensitive Precursor Method. Despite this exceptionally low thermal budget, a remanent polarization, Pr, of 2.8 mC cm_2 was obtained for these BFO films, with a coercive field, Ec, of 380 kV cm_1. In addition, and of significant relevance, the films exhibited a room temperature ferromagnetic response, showing for the first time the multiferroic behaviour at room temperature of BFO films prepared at 300 1C. The ferroelectric, piezoelectric and ferromagnetic functionalities demonstrated for these films revealed their potential for applications in microelectronic devices as well as their feasibility for being used in flexible electronics. The results shown here are a proof of concept of the Seeded Photosensitive Precursor Method for the successful integration of lead-free ferroelectric thin films with flexible plastic substrates and have a broad impact in terms of the extended use of functional oxide thin films processed with low thermal schedules.

Introduction

The preparation of functional oxide thin films at very low temperatures over large areas and compatible with low cost and flexible substrates, offers great industrial potential.1 Flexible electronics are becoming crucial for light, small, portable and flexible microelectronic applications.1 The deposition of crystalline complex oxides on polymer and base metals represents an important extension of thin film technology to substrate materials that is more compatible with innovative applications. The intrinsic multifunctionality of ferroelectric thin films make them very attractive for high-performance, flexible electronic devices such as ferroelectric random access memories (FeRAM), sensors, piezoelectric harvesters or photovoltaic solar cells.2–5 However, the integration of functional ferroelectric oxides with flexible polymers has been prevented by the incompatibility of the respective processing conditions: the polymer is unable to withstand the high temperatures required for electrical response development in the perovskite oxides; for example, most of the synthesis methods require temperatures that exceed 600 1C, 700 1C and 650 1C to crystallize the perovskite ferroelectric films of PbZr1_xTixO3 (PZT), BaxSr1_xTiO3 (BST) and K0.5Na0.5NbO3 (KNN), respectively.6–8 Normally, polyimide and polyester substrates for applications related to the electronics industry are thermally stable below 450 1C (short dwell time) and 150 1C, respectively. Naturally, this temperature difference inhibits the direct deposition of the inorganic ferroelectric films on polymeric substrates.

Up to now, the most widely investigated method of fabricating ferroelectric thin films on flexible polymeric substrates is transfer printing.9,10 This method is an indirect process: first, inorganic ferroelectric films are deposited on rigid substrates and heat treated at high temperatures and then transferred to flexible substrates through a series of processes, such as etching, peeling off, and printing or laser lift off.11 Although transfer printing has been widely investigated, it is a quite complex and expensive process. Therefore, the direct deposition of inorganic ferroelectric films on flexible substrates is in high demand.

Solution-based processes are very attractive for the preparation of functional oxide thin films owing to their wide range of advantages, such as large-area deposition, easy control of composition, atmospheric processing, and low cost (due to the lack of sophisticated instrumentation). Among them, chemical solution deposition (CSD) has been widely used to obtain crystalline thin films at relatively low temperatures. Several attempts to reduce the thin film growth temperatures using different or modifications of CSD-based techniques, such as ultraviolet (UV) assisted annealing,12 laser or microwave heating,13,14 seeding15 and

heterogeneous photocatalysis,16 to levels that are compatible with temperaturesensitive substrates (300–400 1C) have been carried out.

With respect to materials, in recent decades, multiferroic BFO have attracted remarkable research interest due to their large switchable polarization, resistive switching and magnetoelectric properties.17–19 These functionalities are crucial for applications in electronic devices and therefore BFO and its solid solutions hold great potential for applications in spintronics and memory devices.20 The optical bandgap of BFO in the visible range is interesting for applications utilising photoconductivity (sensors), the photovoltaic effect (solar energy harvesting) or photocatalytic performance for use in environmental waste management.21–23

To date, BFO thin films have been deposited mainly on single crystal substrates, with SrTiO3 and DyScO3 being mostly used for the growth of epitaxial BFO films, or on platinized silicon wafers in the case of polycrystalline ones.24–27 From the application point of view, these substrates are expensive and rigid. Moreover other limitations of Bi-based compounds are related to the high annealing temperatures necessary for the crystallization of the perovskite phase and the consequent volatilization of the high-vapour pressure elements such as Bi leading as a consequence to the appearance of parasitic phases.28 Recently, BFO thin films were prepared on flexible metallic Ni tapes with La0.5Sr0.5TiO3 buffer layers by chemical solution deposition.29 Although the BFO films were successfully integrated with metallic foils, the reported crystallization temperature (475–550 1C) for these BFO films was well above the temperature that a flexible polymeric substrate could withstand. Nanocrystalline BFO thin films on SrTiO3 single crystals prepared by low temperature atomic layer deposition (ALD) were reported as well. The BFO films were composed of BFO nanocrystals embedded in an amorphous matrix after deposition at 250 1C. The ferroelectric behaviour of these films was assessed by piezoelectric force microscopy and a piezoelectric coefficient of dzz = 4 pm V_1 was reported.30 Low-temperature processing of BFO thin films compatible with flexible polymeric substrates was very recently reported by the photocatalytically assisted decomposition method of metal precursors. The formation of the perovskite phase was achieved at 325 1C, together with the presence of a secondary crystalline Bi2Fe4O9 phase. Local piezoelectric hysteresis loops were obtained to confirm the ferroelectric character of the BFO thin films on flexible plastic substrates. However, no macroscopic ferroelectric or magnetic functionality was presented.16 Indeed, a review of the literature reveals that the crystalline quality required for attaining a macroscopic ferroelectric response in BFO thin films is difficult to achieve for thin films fabricated at temperatures lower than

400 1C. Fig. 1 depicts the reported experimental values of remanent polarization, Pr, as a function of the fabrication temperature for BFO single crystals,31 bulk ceramics32–34 and thin films.24,35–41 It is clear from the graph that the ferroelectric properties of BFO show strong regression as the processing temperature of the thin films decreases.

In this work, by using our own proprietary technique,42 the Seeded Photosensitive Precursor strategy, we directly fabricate BFO thin films on polyimide substrates for flexible electronics, demonstrating macroscopic ferroelectric switching. The proposed solution-based process combines two different approaches: (i) seeded diphasic sol/solution-gel precursors (SDSG) with (ii) photosensitive precursor solutions (PCSD; PhotoChemical Solution Deposition). The first approach (SDSG) introduces crystalline nanoseeds to the precursor solution in order to enlarge the number of nucleation sites leading to a reduction of the crystallization temperature.43 The second approach (PCSD) is based on the synthesis of photosensitive precursors containing UV absorbing species (like b-diketonates) that, after UV irradiation, produce the pyrolysis and oxidation of the organic components of the solution deposited layer, advancing the formation of the M–O–M bonds of the ferroelectric perovskite at low temperatures.44 Our process not only addresses the issue of Bi volatilization at a high temperature, but also enables a facile production of thin films on low melting temperature substrates. This easy, low-cost solution method was used to prepare BFO multiferroic thin films for the first time at 300 1C, a remarkably low temperature of the formation for this complex perovskite oxide.

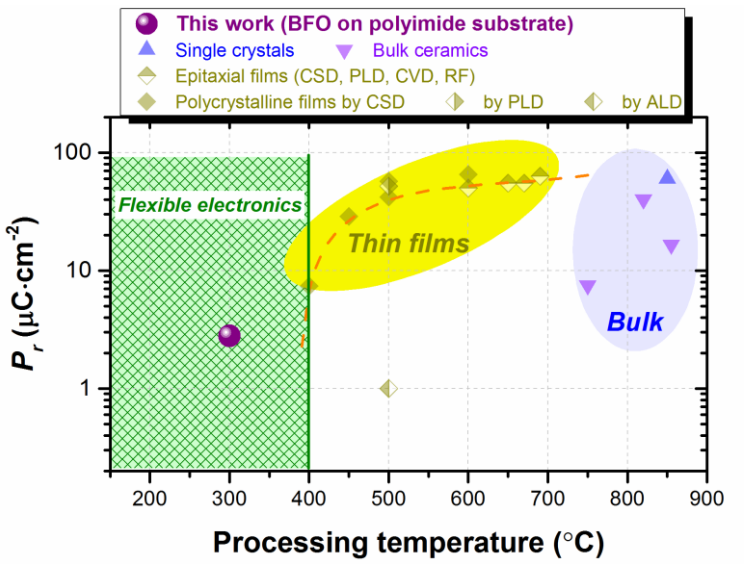

Figure 1. Remanent polarization, Pr, as a function of the BFO single crystals, bulk ceramics and thin film fabrication temperature. Clear regression of the BFO ferroelectric properties is observed for fabrication temperatures lower than 400 1C.

Experimental procedure

Synthesis of precursor solutions and nanosized seeds. 0.25M precursor solution of BFO was prepared using bismuth nitrate ($Bi(NO_3)_3 \cdot 5H_2O$, Sigma Aldrich, 99.99 %) and iron acetylacetonate ($Fe(CH_3COCHCOCH_3)_3$, ABCR, 99 %). Acetic acid ($C_2H_4O_2$ – AcOH, Merck, 100 %) and 1,3-propanediol ($C_3H_8O_2$, Aldrich, 98 %) were used as solvents [44]. No excess of Bi was used. The acetylacetonate ligand of the iron reagent provides an appreciable photosensitivity to this BFO solution [2]. BFO nanopowders to be used as seeds were prepared by hydrothermal method [45]. The chemical regents used to prepare BFO nanoparticles were bismuth nitrate [$Bi(NO_3)_3 \cdot 5H_2O$, Sigma Aldrich, 99.99 %], iron nitrate [$Fe(NO_3)_3 \cdot 9H_2O$, Sigma Aldrich, 98 %], potassium nitrate (KNO_3, Fluka, 98 %), poly(vinyl alcohol) (PVA, Sigma Aldrich, 98 %), and potassium hydroxide (KOH, ABCR, 85 %). The mineralizer-assisted hydrothermal process included the following steps: 0.005 mol $Bi(NO_3)_3 \cdot 5H_2O$ and 0.005 mol $Fe(NO_3)_3 \cdot 9H_2O$ were dissolved in 100 ml of diluted HNO_3 (10 %) to form aqueous solutions. Then, (12M) KOH solution was slowly added to the above solution to adjust its pH value to ~8 by constant stirring until brown precipitates were formed. The precipitates were filtered and washed with distilled water. Then, precipitates were mixed with 30 ml KOH (12 M) and 15 ml PVA (4 g/l) solutions under constant magnetic stirring for 5 min. The suspension solution was transferred into teflon lined stainless-steel autoclaves for the hydrothermal treatment. The autoclave was sealed and kept in the oven at 160 °C for 9 h. The obtained BFO powders were filtered and washed with distilled water and absolute ethanol several times, and then dried at 70 °C for 12 h. The obtained BFO powders were dispersed in a solution of acetic acid and 1,3-propanediol (AcOH:diol, 4:1 vol. ratio). High intensity ultrasonic processor (Vibra Cell 750) was then used to disperse the nanoparticles for 48 h. Suspensions were then left to settle for 3 days to allow sedimentation of the larger particles and aggregates and supernatant were collected. Appropriate volume of seeds suspensions were added to the photoactive BFO precursor to obtain seeded photosensitive precursor solutions.

Preparation of thin films. The method used in this study for the direct fabrication of BFO films onto a polyimide substrate is presented in Figure 2 and consists of the following steps:

- The synthesis of the “photoactive sol”, which displays an increased absorption in the UV-range.

- Incorporation of seeds into the photoactive sol ("seeds + photoactive sol"), that increases the number of nucleation sites in the resulting film producing a further reduction of the crystallization temperature.
- Deposition of seeded photoactive sol on the substrates and irradiation using a high-intensity UV excimer lamp. Elimination of organic compounds from these photosensitive systems is accelerated by the irradiation due to (i) ozonolysis and (ii) a prompt dissociation of the alkyl group–O bonds with subsequent formation of the metal–O–metal bonds.5,44
- Thermal treatment of the irradiated layer by Rapid Thermal Processing (RTP).

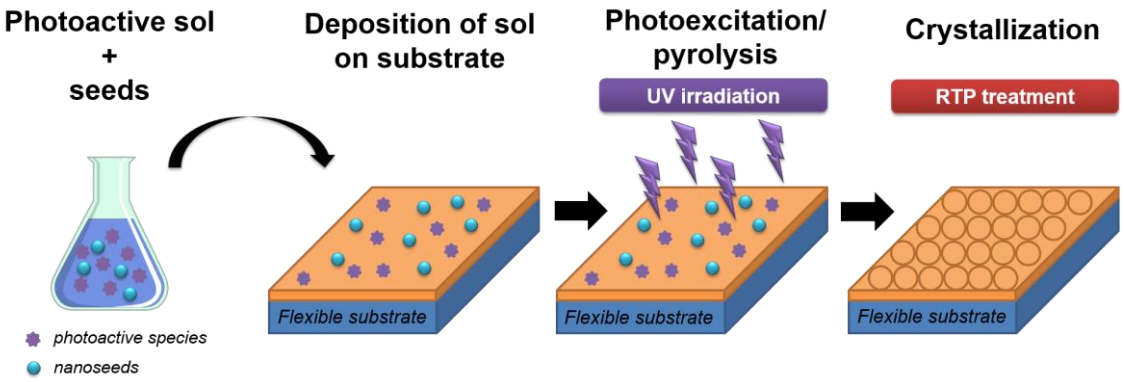

Figure 2. Schematic representation of the strategy that combines seeded diphasic precursors and photochemical solution deposition. This method consists in the preparation of activated sols, deposition of the precursor films, followed by photoexcitation/pyrolysis and final crystallization [4].

Precursor solutions were deposited on flexible polyimide substrates (UPILEX-75S polyimide film; thickness of 75 μm - UBE Europe GmbH). Metallization of the bare polyimide by a NiCr layer with a thickness between 5-10 nm, and a 150-200 nm thick layer of Pt was performed by DC sputtering at room temperature. The deposition of BFO thin films was carried out by spin-coating at 1500 rpm for 45 s.

The as-deposited seeded BFO films were heated on a hot plate in air at 150 1C for 1 min to evaporate the solvents and pyrolyzed at 300 1C for 1 min to burn the residual organics. BFO

thin films prepared by the combination of PCSD and SDSG (denoted as seeded + UV) were dried at 150 1C for 1 min and irradiated using a laboratory-scale prototype combining a

highintensity UV excimer lamp (Heraeus, BlueLight Excimer System, emission = 222 nm, electrical power of 1.5 kW, frequency of 50 Hz, an irradiation length of 30 cm and irradiance of 6.25Wcm_2) with an ultra-fast heating system (Watlow, UltramicTM 600 advanced ceramic heater) under an oxygen atmosphere at 250 1C for 30 min. The deposition and drying steps were repeated 8 times before the RTP annealing to fabricate BFO thin films with the desired thicknesses. The deposited films were crystallised by RTP using the Jetstar 100T JIPELEC equipment. A heating rate of 30 1C s_1 and an air atmosphere were used for film treatments at 300 1C for different periods of time (from 60 to 120 min).

Characterization of materials. X-ray diffraction (XRD) analysis, under Bragg-Brentano (θ/2θ), using a Philips X'Pert, and Bruker D8 T2T SOLX Cu Kα diffractometer were performed to inspect the formed phases in BFO nanoparticles and thin films. Microstructures of BFO thin films were observed with scanning electron microscopy (SEM, Hitachi SU-70). Nanoparticles were analysed by using a Transmission Electron Microscopy (TEM) Hitachi H9000-NA (300 keV). The surface area of the particles, SA_{BET} ($m^2 \cdot g^{-1}$) was evaluated by the Brunauer-Emmett-Teller (BET) method in which N_2 acted as adsorbate gas (Micromeritics Gemini 2375 equipment). Prior to the measurements, the samples were degassed at ~200 ºC for 12 h. Ferroelectric hysteresis behaviour was assessed with a virtual ground circuit. Experimental setup consisted of Agilent 33220A waveform generator that allows the application of sinusoidal waves with electrical amplitude signals between 0.01-16 V and frequencies between 1 kHz and 10 kHz. Current intensity generated values, after amplification with a Keithley 428 current amplifier, together with the voltage applied were collected with a Tektronix TDS 520 oscilloscope. Data acquisition and further processing of the data were carried out with homemade software.46 An AFM system consisting of a commercial NT-MDT NTEGRA Aura scanning probe microscope equipped with Piezoresponce Force Microscopy mode was used. Measurements were carried out using a cantilever Mikromash HQ: NSC35/pt with spring constant of 16 N/m and resonance frequency of 300 kHz. A small ac electric field of 5 V and frequency 70 kHz was applied to the tip to induce local vibration. The topography and domain images were processed using WSxM v2.2 software. A vibrating sample magnetometer (VSM) instrument (Cryogenics, UK) was used to measure the magnetic behaviour of the sample up to 10 T at room temperature. The measurements were made by applying the magnetic field parallel to the surface of the film (in-plane).

Results

Characterization of seeds

The powder morphology, particle size and its dispersion behaviour are equally important for the quality of the seeded films and, consequently determine the final functional properties. The XRD pattern in logarithmic scale of BFO particles to be used as seeds is shown in Figure 3a. The nanoparticles present a single-phase BFO perovskite structure. The diffraction pattern is indexed based on the rhombohedral *R3c* structure (JCPDS #04-009-3445 file). No characteristic XRD peaks of possible impurity phases, such as Fe_2O_3, Bi_2O_3, $Bi_2Fe_4O_9$, $Bi_{25}FeO_{40}$ or $Bi_{36}Fe_{24}O_{57}$ were observed within the resolution of XRD.

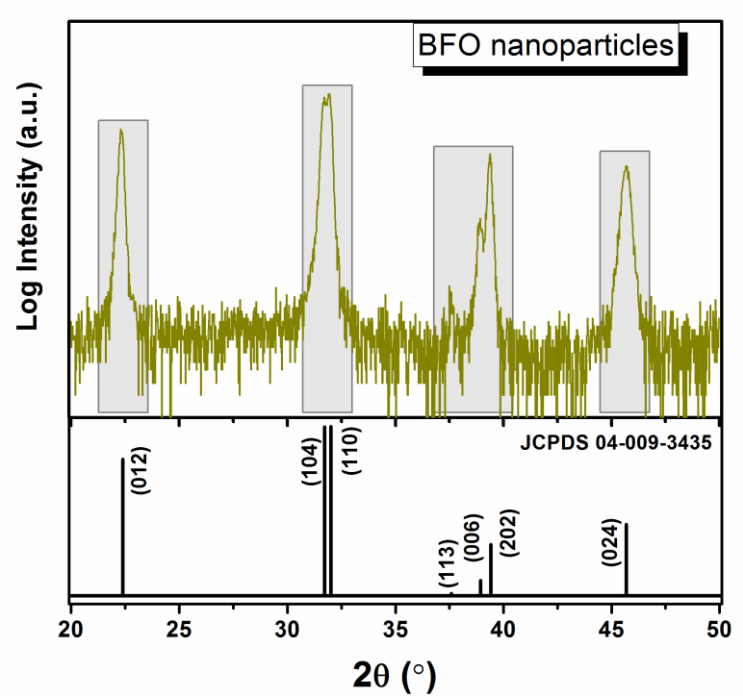

a)

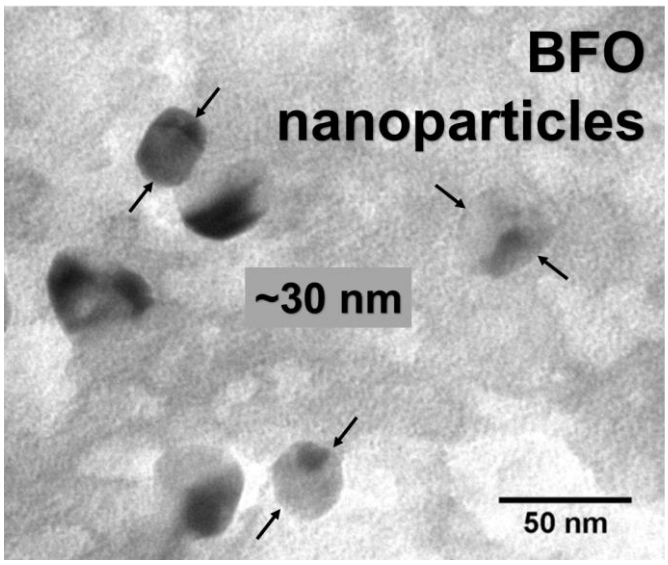

b)

c)

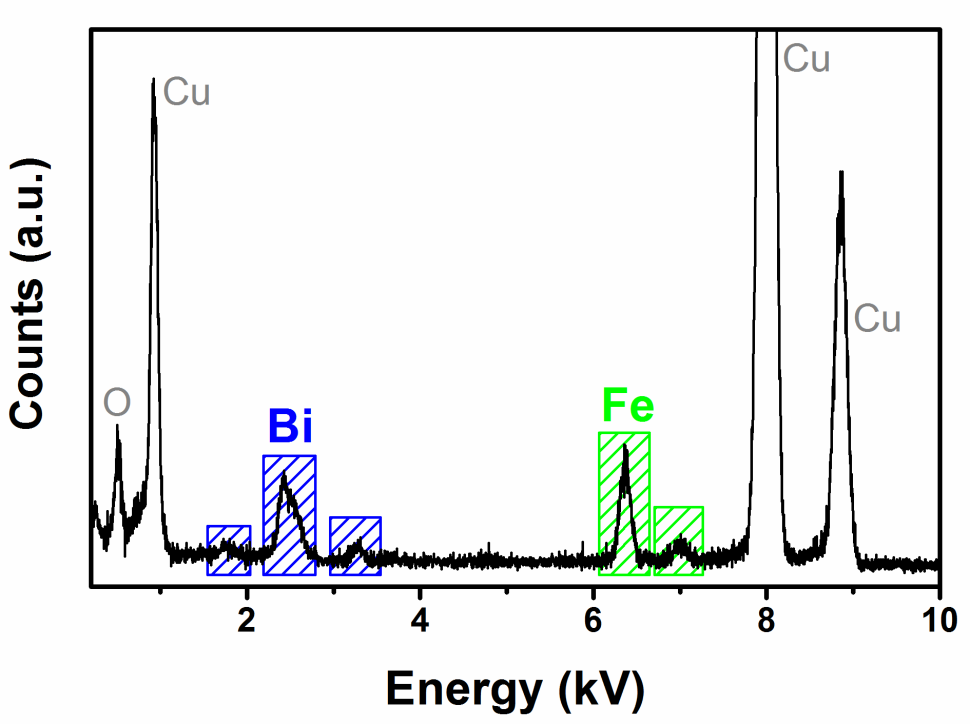

Figure 3. XRD pattern (a), TEM bright field image (b) and EDS spectra (c) of BFO nanoseeds synthesized by the hydrothermal process. BFO nanoparticles present a single-phase perovskite structure and ultra-fine spherical morphology with the average particle size of about 30 nm.

The mean particle size of the powders (D) was also calculated from the specific surface area of BET, as $D_{BET} = 6000/S_{BET} \cdot \rho$, in which S_{BET} stands for the specific area (m^2/g) and ρ for the theoretical density (g/cm^3). The measured value of S_{BET} was 25.19 m^2/g. Fine-grained powders have particularly high surface areas owing to small particle sizes. The mean particle size D_{BET} calculated assuming spherical particle morphology is ~29 nm for these BFO nanopowders. For comparison the specific surface area reported for BFO particles prepared by classical solid state reaction is S_{BET} ~ 4.25 m^2/g, that correspond to average particles size of 15 µm [46]. The morphology of the powders disaggregated by sonication was studied by TEM and is shown in Figure 3b. Ultra-fine spherical BFO powder particles with an original particle size of about 30 nm were obtained. This is consistent with the average size calculated from S_{BET}. To confirm the chemical composition of these as-prepared structures, energy dispersive X-ray spectroscopy (EDS) spectra (Figure 3c), taken at a number of selected positions of the sample, show the expected presence of Bi, Fe, and O. Copper signal detected by EDX comes from the used supporting grid.

Characterization of thin films

BFO films prepared on the flexible polyamide substrates present a very uniform aspect, they are adherent to the substrate and when bended they do not crack, as presented in Figure 4a.

XRD patterns of BFO thin films processed at 300 °C are presented in Figure 4b. No evidence of crystallinity (i.e., amorphous BFO film) is observed in the diffractogram of *unseeded* films after annealing at 300 ºC. The diffraction peaks for the *seeded* and *seeded+UV* BFO films may be indexed according to either the electrode or a rhombohedrally ((JCPDS #04-009-3445 file) distorted perovskite structure of BFO. Similarly, to our studies on PZT thin films, the BFO seeds distributed in the amorphous BFO layers act as preferential nucleation sites, and the perovskite phase formation is promoted at lower temperature in contrast to the films without seeds [4, 47].

a)

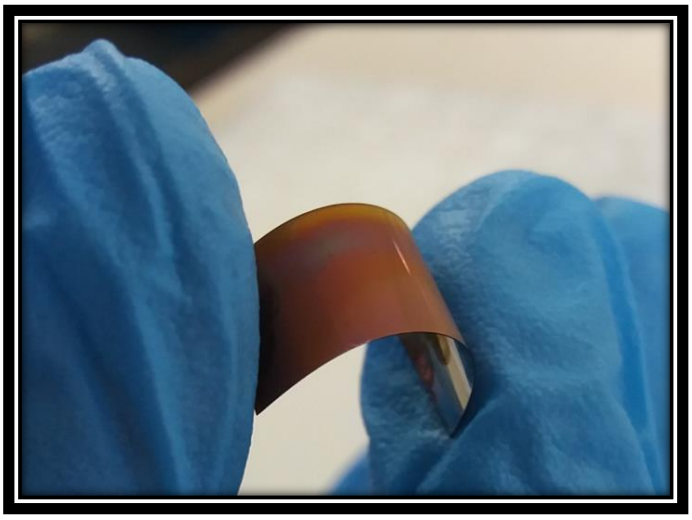

b)

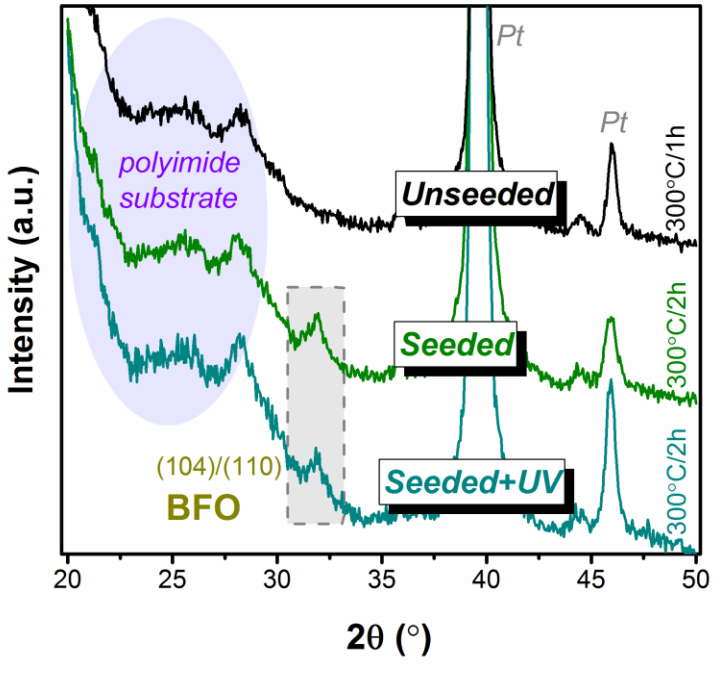

Figure 4. (a) Photograph of a flexible BFO film fabricated on polyamide substrate. (b) XRD patterns of BFO thin films processed at 300 °C on flexible substrates. *Unseeded* films are amorphous. Reflections corresponding to the perovskite phase are detected for *seeded* and *seeded+UV* BFO films.

The surface morphologies of the crystalline seeded and seeded + UV BFO films were inspected by SEM. Typical micrographs are shown in Fig. 5. All fabricated BFO films are crack free and composed of fine and densely compacted grains. The morphology of the films consists of nanosized grains with a mean diameter of B70 and B100 nm for the seeded and seeded + UV BFO thin films, respectively.

a)

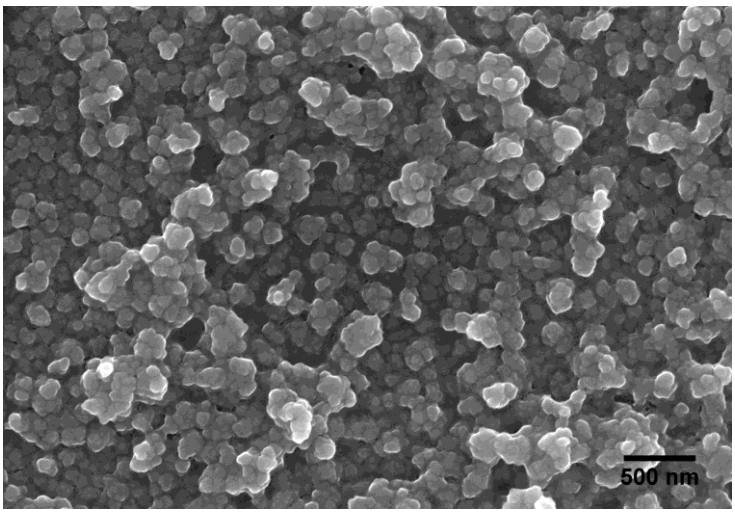

b)

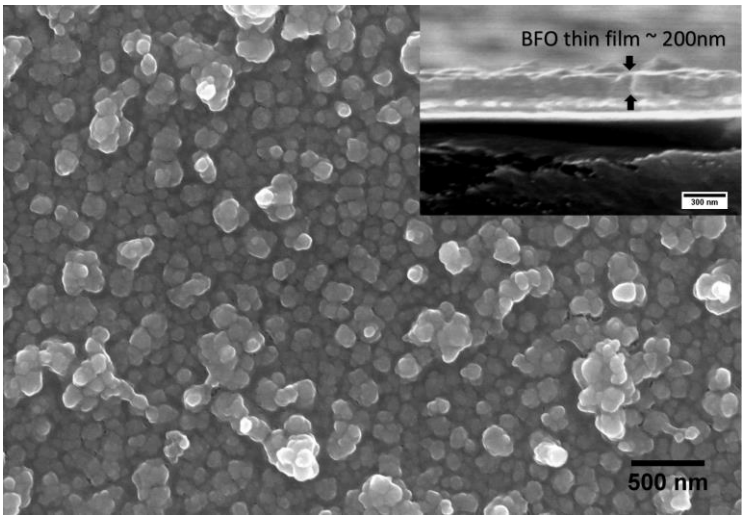

Figure 5. SEM micrographs of *seeded* (a) and *seeded and UV irradiated* (b) of BFO thin films on flexible polyamide substrate. The morphology of the films consists of nanosized grains with a mean diameter of ~70 and ~100 nm for *seeded* and *seeded+UV* BFO thin films, respectively.

Moreover, the surface of the films is compact but rather rough, quantified later by AFM. From the inset in Fig. 5b, we can see that films possess uniform thickness along the substrate and the thickness is about 200 nm.

The ferroelectric hysteresis curves measured at 140 K in *seeded* and *seeded+UV* BFO films are illustrated in Figure 6. Despite the low thermal budget that affects the crystal quality and microstructure of the films a remanent polarization P_r of 2.8 μC/cm^2 is obtained for the *seeded+UV f*ilm, with a coercive field *Ec* of 300 kV/cm, which confirms the ferroelectric nature of the perovskite phase prepared at only 300 ºC. Polarization current peaks can clearly be seen when the applied field reaches *Ec*. This is a clear evidence of ferroelectric domain switching. (Figure 6b) [50]. In the case of *seeded* films an appreciable lower remanent polarization P_r of 1 μC/cm^2 is obtained.

The local piezoelectric behaviour of seeded and seeded + UV BFO films was investigated using vertical piezoresponse force microscopy (VPFM). Fig. 7 shows the simultaneously recorded topography and VPFM amplitude and phase responses with an ac bias (5 V, 70 kHz) applied to the tip. The topography of the ferroelectric BFO thin films shows small grains with diameters ofB75 andB100 nm for the seeded and seeded + UV BFO thin films consistent with the SEM micrographs. The RMS roughness of the seeded-only and seeded and UV-irradiated films were RRMS = 40.8 _ 3.8 nm and RRMS = 49.8 _ 5.8 nm, respectively. The dark areas in the VPFM phase images correspond to domains in which the polarization is oriented in the opposite direction to the applied field (phase = _1801), while the bright regions correspond to domains with the polarization oriented along the applied field (phase = 1801). The VPFM phase image is characterized by a strong domain contrast, and the domains are mostly confined within grain boundaries: deep bright and dark areas indicate significant out-of-plane components of polarization. There is also a fraction of regions with poor contrast (indicated by the blue dashed line in Fig. 7), likely corresponding to areas of the films with incipient crystallization and domains with in-plane polarization. The VPFM amplitude and phase images of seeded + UV BFO films show that the piezoelectric domains in these films are bigger than those in the case of the seeded BFO films (highlighted in green for comparison in Fig. 7). The average domain sizes for the seeded and seeded + UV BFO films were measured to be 60 nm and 100 nm, respectively; the domain size was estimated from the VPFM phase line profiles. However, the marked domains in the VPFM phase images of seeded + UV BFO films show sizes bigger than 200 nm because neighbouring grains merge into one domain.

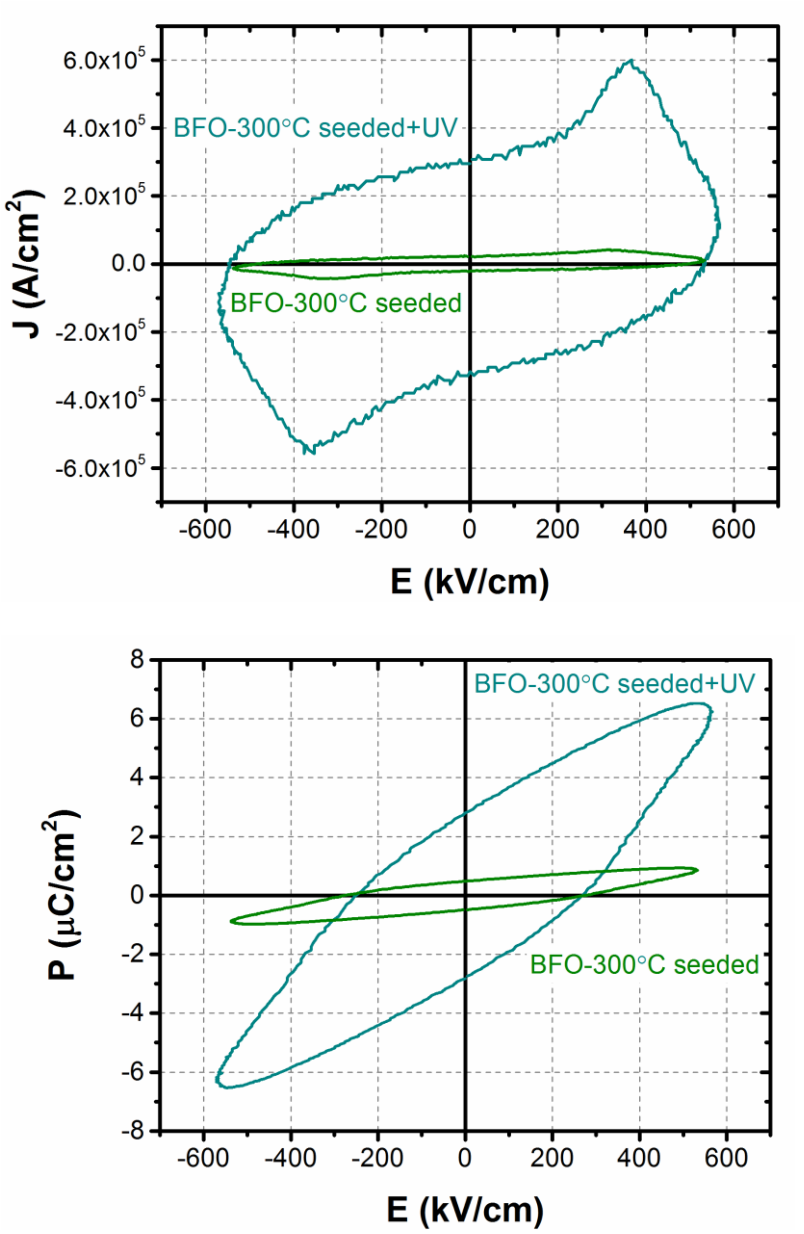

Figure 6. The polarization (P-E) hysteresis loops (a) and the switching currents versus applied field (b), for *seeded* and *seeded and UV-irradiated* BFO films measured at 140 K and ~~at~~ 10 kHz. A remanent polarization P_r of 2.8 μC/cm^2 is obtained for the *seeded*+ *UV* ~~*irradiated*~~ film, with a coercive field *Ec* of 300 kV/cm confirm the ferroelectric nature of the perovskite phase prepared at only 300 ºC.

The magnetic behaviour of the BFO thin films was assessed at room temperature and is displayed in Fig. 8. M–H hysteresis curves of the BFO films on flexible polyimide substrates depict unsaturated hysteresis loops, with weak ferromagnetic behaviour with a small coercivity (2Hc) of 200 Oe for the seeded + UV BFO films (represented as an inset of Fig. 8).

Discussion

The results shown above clearly demonstrate the crystallization enhancement and fine-grained morphology development with nanosized grains of the seeded and seeded + UV BFO films compared with unseeded ones (Fig. 4 and 5).

BFO seeds distributed in the amorphous BFO layers act as preferential nucleation sites, and the perovskite phase formation is promoted at lower temperatures in contrast with the films without seeds, similar to our studies on PZT thin films.[49,50] The presence of nanometric BFO seeds in the films lowers the barrier for BFO nucleation and these perovskite nanoseeds act as preferential nucleation sites within the amorphous films, which result in a large number of small and equiaxed grains. It is well documented that the small grain size in thin films indicates a high nucleation rate.[51,52] In addition, UV irradiation causes the electronic excitation of particular chemical bonds in seeded amorphous films, which enhances the decomposition of the metal precursors, therefore promoting crystallization of the oxide phase at lower temperatures.[5,44] The photoactivation by UV irradiation of seeded amorphous films enhances the pyrolysis and elimination of organic components in these films, which further promotes the grain growth at an earlier stage. Consequently, slightly bigger grains were observed for the seeded + UV BFO thin films.

It is well known that the electrical properties of ferroelectric films depend on several factors, which include phase purity, microstructure, crystallite orientation, stresses, grain size or imperfections such as charged defects and vacancies.[53] Therefore, the enhanced crystallinity and microstructure of seeded and seeded + UV BFO films are expected to have a direct influence on their electrical and magnetic response; indeed, we also expect these films to be less defective. In particular, UV-irradiation of oxide layers under an oxygen atmosphere was shown to lead to the formation of ozone (O3), a strong oxidant agent, and monoatomic oxygen O(1D), which reacts with sub-oxides, improving the stoichiometry and decreasing defects.[54–56]

The average domain sizes for seeded and seeded + UV BFO films were measured by PFM to be 60 nm and 100 nm, respectively. This fact is a consequence of the higher crystallinity present in the films prepared by a strategy that combines seeded precursors and UV-irradiation of the photoactive deposited layers (seeded photosensitive precursor method). This increase in the domain size points toward the enhancement of the ferroelectric polarization. Indeed, this local observation at the nanoscale is consistent with the macroscopic P–E loops

results (Fig. 7). Much better defined macroscopic hysteresis loops were observed for seeded + UV BFO films rather than seeded-only BFOs (Fig. 6). Moreover, the increased Pr of the seeded + UV films can be attributed to the decrease in the density of defects and oxygen vacancies.

BFO is known to show a G-type antiferromagnetic ordering. In bulk BFO, a small net magnetization due to the canting of adjacent Fe3+ spins is modulated by a long-range superstructure superimposed on the spin arrangement. The net magnetic moment is cancelled out due to the magnetization rotation following a cycloid with B62 nm periodicity.31 In nanocrystalline BFO thin films and nanoparticles smaller than 95 nm, BFO shows a ferromagnetic behaviour due to incomplete rotation of the spins along the antiferromagnetic axis.57,58 This weak ferromagnetism can appear in nanocrystalline BiFeO3 due to surface defects, lattice strain, the presence of Fe2+ in the nanomaterials because of oxygen deficiency, etc.57 It is clear from the SEM micrographs of these BFO films that the BFO grains are smaller than 100 nm; therefore, the cycloid-like magnetic modulation was broken or significantly distorted in our films, leading to this weak ferromagnetic behaviour. This is a very important result showing for the first time the multiferroic behaviour at room temperature of BFO films prepared at 300 1C (Fig. 8).

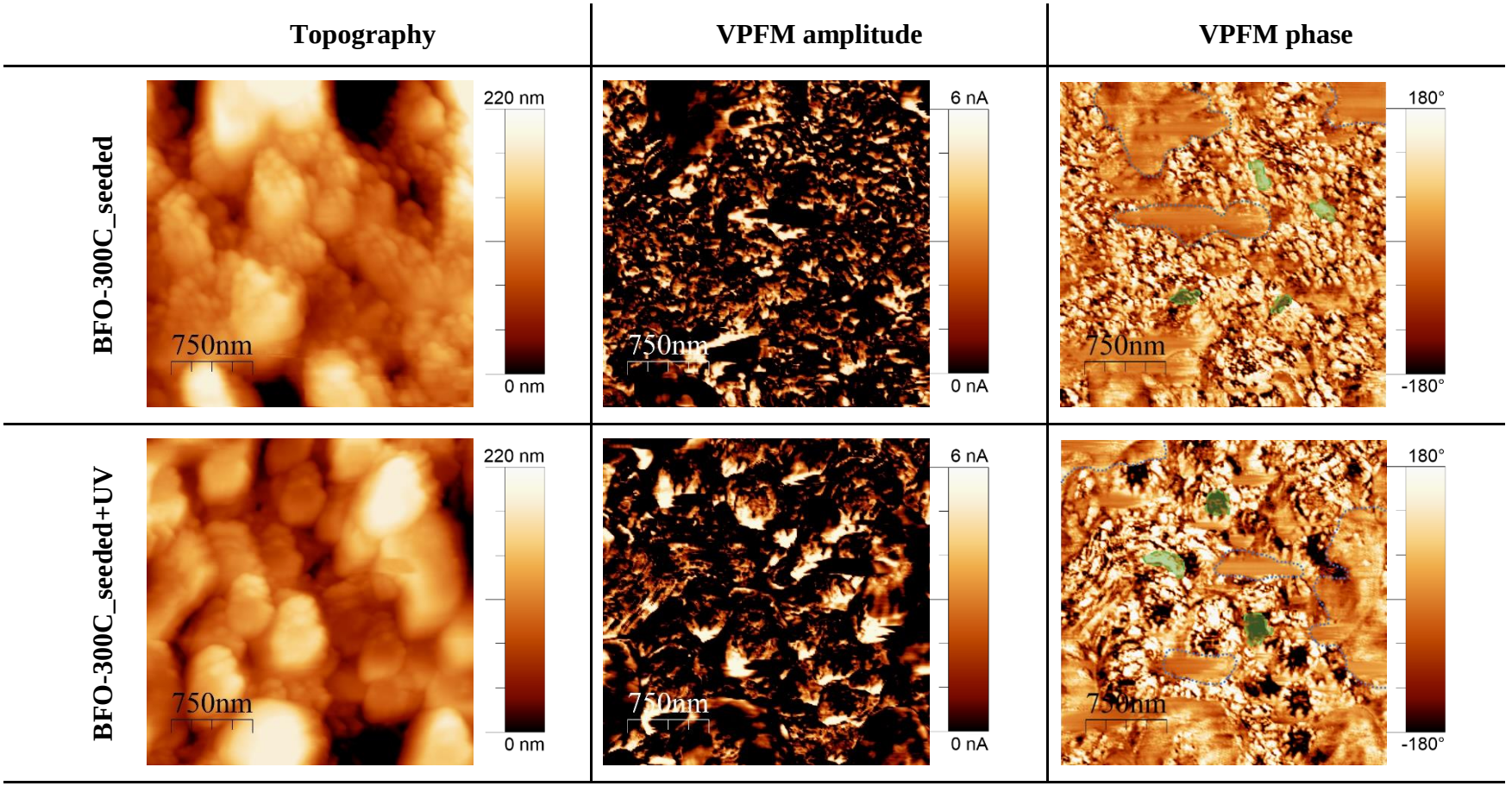

Figure 7. Topographic and VPFM amplitude and phase images of *seeded* and *seeded+UV*- BFO thin films on flexible polyimide substrates crystalized at 300 °C for 120 min. Both films depict obvious piezoelectric behaviour, however areas with poor contrast, indicated by blue dashed line, likely correspond to regions of the films with incipient crystallization and domains with in-plane polarization. Some of the domains are highlighted in green for comparison.

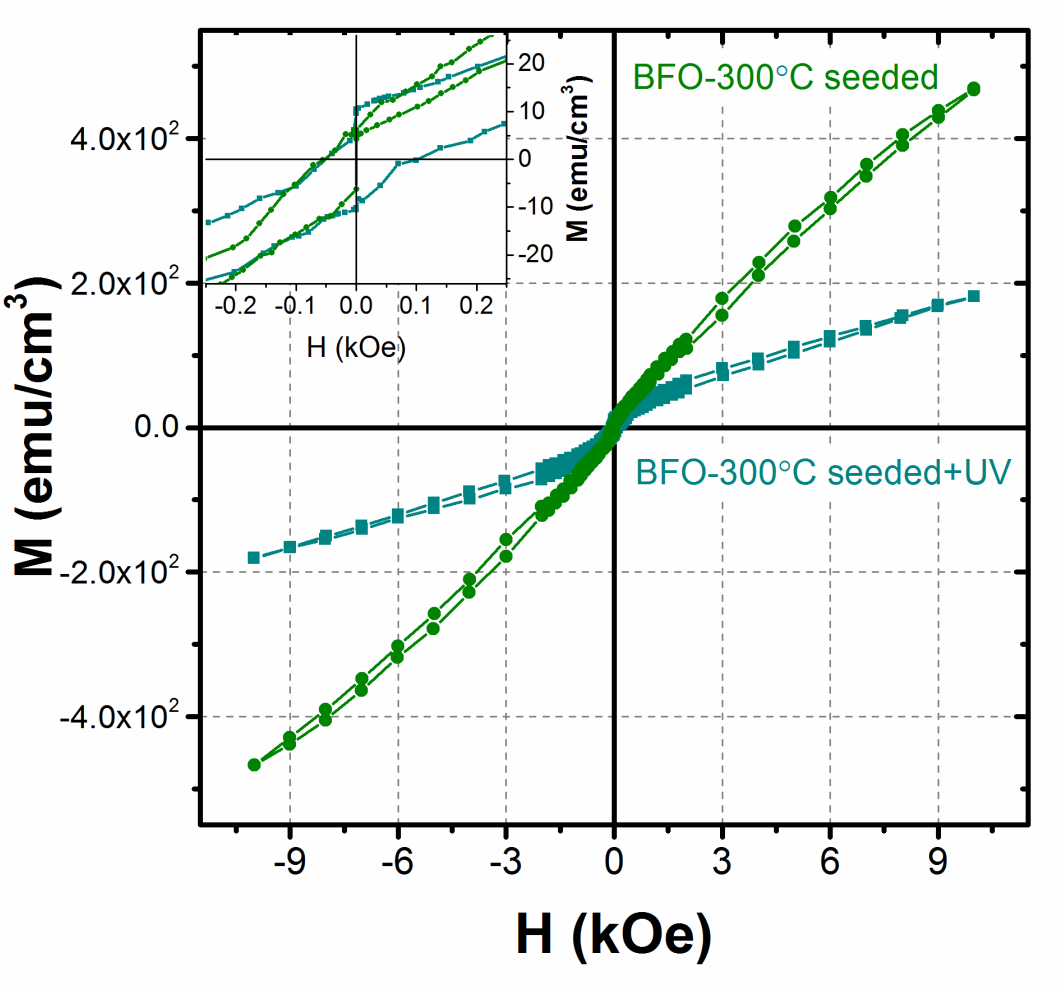

Figure 8. Magnetic hysteresis of *seeded* and *seeded+UV* BFO at 300 K up to 10 kOe. BFO on flexible polyimide substrates depict the weak ferromagnetic response. The magnetic response increases with decreasing grain size of BFO thin films.

Conclusions

Here, we prove that it is possible to directly fabricate lead-free BFO thin films on flexible polyimide substrates with ferroelectric and magnetic functionalities (multiferroicity) at room temperature. Our own proprietary novel solution-based Seeded Photosensitive Precursor Method was successfully used to decrease the crystallization temperature of BFO thin films to as low as 300 1C, the lowest reported temperature to date for the preparation of multiferroic BFO thin films. Regardless of this exceptionally low thermal budget, these seeded +UV BFO films present a remanent polarization Pr of 2.8 mC cm_2, a coercive field Ec of 380 kV cm_1 (Fig. 1) and notably exhibit a room temperature ferromagnetic response, corresponding to a broken or significantly distorted cycloid-like magnetic modulation, showing for the first time

the multiferroic behaviour at room temperature of BFO films prepared at 300 1C. The synthesis strategy based on the use of seeded photosensitive precursors can be transferred to any family of functional metal oxides. This concept allows the direct fabrication of complex oxide thin films on polyimide substrates targeted for flexible and miniaturized electronic components to produce light, low cost, low power consumption, and portable electronic devices.

Acknowledgments

This work was developed within the scope of the project CICECO-Aveiro Institute of Materials, POCI-01-0145-FEDER-007679 (FCT Ref. UID/CTM/50011/2013), financed by Portuguese funds through the FCT/MEC and, when appropriate, co-financed by FEDER under the PT2020 Partnership Agreement. The work has also been partially financed by the Spanish Project MAT2016-76851- R. M. T. acknowledges FCT for financial support (SFRH/BD/81123/ 2011). I. B. acknowledges financial support from Fundación General CSIC (Spanish ComFuturo Programme). The authors acknowledge COST Action IC1208 for funding the Short Term Scientific Mission of M. T. at the ICMM-CSIC.

References:

1. Wu, A., et al., *Early Stages of Crystallization of Sol−Gel-Derived Lead Zirconate Titanate Thin Films.* Chemistry of Materials, 2003. **15**(5): p. 1147-1155.
2. Calzada, M.L., et al., *Low-Temperature Processing of Ferroelectric Thin Films Compatible with Silicon Integrated Circuit Technology.* Advanced Materials, 2004. **16**(18): p. 1620-1624.
3. Vilarinho, P.M., et al., *Method for the preparation at low temperatures of ferroelectric thin films, the ferroelectric thin films thus obtained and their applications*, 2013.
4. Bretos, I., et al., *Activated Solutions Enabling Low-Temperature Processing of Functional Ferroelectric Oxides for Flexible Electronics.* Advanced Materials, 2014. **26**(9): p. 1405-1409.
5. Nathan, A., et al., *Flexible Electronics: The Next Ubiquitous Platform.* Proceedings of the IEEE, 2012. **100**(Special Centennial Issue): p. 1486-1517.
6. Setter, N., et al., *Ferroelectric Thin Films: Review of Materials, Properties, and Applications.* Journal of Applied Physics, 2006. **100**(5): p. 051606-46.
7. Bowen, C.R., et al., *Piezoelectric and ferroelectric materials and structures for energy harvesting applications.* Energy & Environmental Science, 2014. **7**(1): p. 25-44.
8. Yuan, Y., et al., *Arising applications of ferroelectric materials in photovoltaic devices.* Journal of Materials Chemistry A, 2014. **2**(17): p. 6027-6041.
9. González, M.B., A. Wu, and P.M. Vilarinho, *Influence of Solvents on the Microstructure and Dielectric Properties of Ba0.5Sr0.5TiO3 Thin Films Prepared by a Diol-Based Sol−Gel Process.* Chemistry of Materials, 2006. **18**(7): p. 1737-1744.

10. Izyumskaya, N., et al., *Processing, Structure, Properties, and Applications of PZT Thin Films.* Critical Reviews in Solid State and Materials Sciences, 2007. **32**(3-4): p. 111-202.
11. Yu, Q., et al., *Effect of Pyrolysis Temperature on Sol–Gel Synthesis of Lead-free Piezoelectric (K,Na)NbO_3 Films on Nb:$SrTiO_3$ Substrates.* Journal of the American Ceramic Society, 2014. **97**(1): p. 107-113.
12. Qi, Y., et al., *Piezoelectric Ribbons Printed onto Rubber for Flexible Energy Conversion.* Nano Letters, 2010. **10**(2): p. 524-528.
13. Rho, J., et al., *$PbZr_xTi_{1-x}O_3$ Ferroelectric Thin-Film Capacitors for Flexible Nonvolatile Memory Applications.* IEEE Electron Device Letters, 2010. **31**(9): p. 1017-1019.
14. Do, Y.H., et al., *Preparation on transparent flexible piezoelectric energy harvester based on PZT films by laser lift-off process.* Sensors and Actuators A: Physical, 2013. **200**: p. 51-55.
15. Nakajima, T., K. Shinoda, and T. Tsuchiya, *UV-assisted nucleation and growth of oxide films from chemical solutions.* Chemical Society Reviews, 2014. **43**(7): p. 2027-2041.
16. Wang, Z.J., et al., *Low-temperature growth of high-quality lead zirconate titanate thin films by 28 GHz microwave irradiation.* Applied Physics Letters, 2005. **86**(21): p. 212903.
17. Bharadwaja, S.S.N., et al., *Excimer Laser Crystallized (Pb,La)(Zr,Ti)O_3 Thin Films.* Journal of the American Ceramic Society, 2008. **91**(5): p. 1580-1585.
18. Wu, A., et al., *Processing and Seeding Effects on Crystallisation of PZT Thin Films from Sol-Gel Method.* Journal of the European Ceramic Society, 1997. **17**(12): p. 1443-1452.
19. Bretos, I., et al., *Low-Temperature Liquid Precursors of Crystalline Metal Oxides Assisted by Heterogeneous Photocatalysis.* Advanced Materials, 2015. **27**(16): p. 2608-2613.
20. Lebeugle, D., et al., *Very Large Spontaneous Electric Polarization in $BiFeO_3$ Single Crystals at Room Temperature and its Evolution Under Cycling Fields.* Applied Physics Letters, 2007. **91**(2): p. 022907-3.
21. Yin, K., et al., *Resistance switching in polycrystalline $BiFeO_3$ thin films.* Applied Physics Letters, 2010. **97**(4): p. 042101.
22. Zvezdin, A.K., et al., *Magnetoelectric interaction and magnetic field control of electric polarization in multiferroics.* Journal of Magnetism and Magnetic Materials, 2006. **300**(1): p. 224-228.
23. Ramesh, R. and N.A. Spaldin, *Multiferroics: progress and prospects in thin films.* Nat Mater, 2007. **6**(1): p. 21-29.
24. Gao, F., et al., *Visible-Light Photocatalytic Properties of Weak Magnetic BiFeO3 Nanoparticles.* Advanced Materials, 2007. **19**(19): p. 2889-2892.
25. Basu, S.R., et al., *Photoconductivity in $BiFeO_3$ thin films.* Applied Physics Letters, 2008. **92**(9): p. 091905.
26. Choi, T., et al., *Switchable Ferroelectric Diode and Photovoltaic Effect in $BiFeO_3$.* Science, 2009. **324**(5923): p. 63-66.
27. Wang, J., et al., *Epitaxial $BiFeO_3$ Multiferroic Thin Film Heterostructures.* Science, 2003. **299**(5613): p. 1719-1722.
28. Ueno, R., et al., *Crystal Structure and Electrical Properties of Epitaxial $BiFeO_3$ Thin Films Grown by Metal Organic Chemical Vapor Deposition.* Japanese Journal of Applied Physics, 2005. **44**(9L): p. L1231.
29. Lee, C.-C. and J.-M. Wu, *Effect of film thickness on interface and electric properties of $BiFeO_3$ thin films.* Applied Surface Science, 2007. **253**(17): p. 7069-7073.

30. Zhang, Q., N. Valanoor, and O. Standard, *Chemical solution deposition derived (001)-oriented epitaxial $BiFeO_3$ thin films with robust ferroelectric properties using stoichiometric precursors (invited).* Journal of Applied Physics, 2014. **116**(6): p. 066810.
31. Tyholdt, F., et al., *Synthesis of Oriented $BiFeO_3$ Thin Films by Chemical Solution Deposition: Phase, Texture, and Microstructural Development.* Journal of Materials Research, 2005. **20**(08): p. 2127-2139.
32. Tang, X., et al., *$BiFeO_3$ thin films prepared on metallic Ni tapes by chemical solution deposition: effects of annealing temperature and a $La_{0.5}Sr_{0.5}TiO_3$ buffer layer on the dielectric, ferroelectric and leakage properties.* RSC Advances, 2014. **4**: p. 32738–32743.
33. Coll, M., et al., *Nanocrystalline Ferroelectric $BiFeO_3$ Thin Films by Low-Temperature Atomic Layer Deposition.* Chemistry of Materials, 2015. **27**(18): p. 6322-6328.
34. Lebeugle, D., et al., *Room-temperature coexistence of large electric polarization and magnetic order in $BiFeO_3$ single crystals.* Physical Review B, 2007. **76**(2): p. 024116.
35. Yuan, G.L., et al., *Preparation and multi-properties of insulated single-phase BiFeO3 ceramics.* Solid State Communications, 2006. **138**(2): p. 76-81.
36. Shvartsman, V.V., et al., *Large Bulk Polarization and Regular Domain Structure in Ceramic $BiFeO_3$.* Applied Physics Letters, 2007. **90**(17): p. 172115-3.
37. Song, S.H., et al., *A comparative study of dielectric, ferroelectric and magnetic properties of $BiFeO_3$ multiferroic ceramics synthesized by conventional and spark plasma sintering techniques.* Journal of the European Ceramic Society, 2015. **35**(1): p. 131-138.
38. Singh, S.K., et al., *Epitaxial $BiFeO_3$ thin films fabricated by chemical solution deposition.* Applied Physics Letters, 2006. **88**(16): p. 162904.
39. Das, R.R., et al., *Synthesis and ferroelectric properties of epitaxial $BiFeO_3$ thin films grown by sputtering.* Applied Physics Letters, 2006. **88**(24): p. 242904.
40. Yang, S.Y., et al., *Metalorganic chemical vapor deposition of lead-free ferroelectric $BiFeO_3$ films for memory applications.* Applied Physics Letters, 2005. **87**(10): p. 102903.
41. Chung, J.-K., et al., *The characteristics of $BiFeO_3$ multiferroic thin films grown by pulsed laser deposition* Integrated Ferroelectrics, 2007. **87**(1): p. 25-32.
42. Liu, Y.-T., et al., *Ultrathin Oriented $BiFeO_3$ Films from Deposition of Atomic Layers with Greatly Improved Leakage and Ferroelectric Properties.* ACS Applied Materials & Interfaces, 2014. **6**(1): p. 443-449.
43. Jin, L., et al., *$BiFeO_3$(00l)/$LaNiO_3$/Si thin films with enhanced polarization: an all-solution approach.* RSC Advances, 2016. **6**(82): p. 78629-78635.
44. Perez-Rivero, A., et al., *Polarization switching at room temperature of undoped $BiFeO_3$ thin films crystallized at temperatures between 400 < T < 500C.* Journal of Materials Science: Matererials in Electronics, 2015. **26**: p. 9373-9386.
45. Wang, Y., et al., *Low temperature polymer assisted hydrothermal synthesis of bismuth ferrite nanoparticles.* Ceramics International, 2008. **34**(6): p. 1569-1571.
46. Farhadi, S. and N. Rashidi, *Perovskite-type ferromagnetic $BiFeO_3$ nanopowder: a new magnetically recoverable heterogeneous nanocatalyst for efficient and selective transfer hydrogenation of aromatic nitro compounds into aromatic amines under microwave heating.* Journal of the Iranian Chemical Society, 2012. **9**(6): p. 1021-1031.
47. Bretos, I., et al., *Active layers of high-performance lead zirconate titanate at temperatures compatible with silicon nano- and microelectronic devices.* Scientific Reports, 2016. **6**: p. 20143.

48. Wu, A., et al., *Kinetic Aspects of the Formation of Seeded Lead Zirconate Titanate Thin Films.* Integrated Ferroelectrics, 2000. **30**(1-4): p. 261-270.
49. Voigt, J.A., et al., *Oriented Lead Zirconate Titanate thin Films: Characterization of Film Crystallization.* MRS Proceedings, 1993. **310**.
50. Yan, H., et al., *The contribution of electrical conductivity, dielectric permittivity and domain wsitching in ferroelectric hysteresis loops* Journal of Advanced Dielectrics, 2011. **01**(01): p. 107-118.
51. Shaw, T.M., S. Trolier-McKinstry, and P.C. McIntyre, *The Properties of Ferroelectric Films at Small Dimensions.* Annual Review of Materials Science, 2000. **30**(1): p. 263-298.
52. Park, T.-J., et al., *Size-Dependent Magnetic Properties of Single-Crystalline Multiferroic $BiFeO_3$ Nanoparticles.* Nano Letters, 2007. **7**(3): p. 766-772.
53. Marchand, B., et al., *Electric and Magnetic Properties of ALD-Grown $BiFeO_3$ Films.* The Journal of Physical Chemistry C, 2016. **120**(13): p. 7313-7322.
54. Huang, F., et al., *Peculiar magnetism of $BiFeO_3$ nanoparticles with size approaching the period of the spiral spin structure.* Scientific Reports, 2013. **3**: p. 2907.